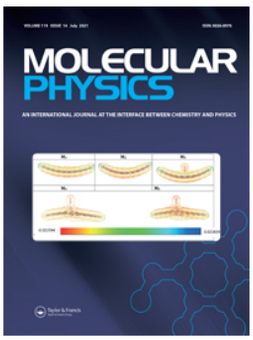

Taylor & Francis
Taylor & Francis Group

Molecular Physics

An International Journal at the Interface Between Chemistry and Physics

ISSN: (Print) (Online) Journal homepage: https://www.tandfonline.com/loi/tmph20

# Controlled preparation and vibrational excitation of single ultracold molecular hydrogen ions

Christian Wellers, Magnus R. Schenkel, Gouri S. Giri, Kenneth R. Brown & Stephan Schiller

**To cite this article:** Christian Wellers, Magnus R. Schenkel, Gouri S. Giri, Kenneth R. Brown & Stephan Schiller (2021): Controlled preparation and vibrational excitation of single ultracold molecular hydrogen ions, Molecular Physics, DOI: 10.1080/00268976.2021.2001599

**To link to this article:** https://doi.org/10.1080/00268976.2021.2001599

Published online: 17 Nov 2021.

MOLECULAR PHYSICS e2001599
https://doi.org/10.1080/00268976.2021.2001599

Taylor & Francis
Taylor & Francis Group

L. WOLNIEWICZ SPECIAL ISSUE



# Controlled preparation and vibrational excitation of single ultracold molecular hydrogen ions

Christian Wellers [a], Magnus R. Schenkel [a], Gouri S. Giri [a], Kenneth R. Brown [b] and Stephan Schiller [a]

[a]Institut für Experimentalphysik, Heinrich-Heine-Universität Düsseldorf, Düsseldorf, Germany; [b]Departments of Electrical and Computer Engineering, Duke University, Durham, NC, USA

**ABSTRACT**

A single, trapped and ultracold molecular hydrogen ion is an attractive quantum system for exploring various aspects of fundamental physics, such as the determination of fundamental constants and testing their time-independence. Here we demonstrate, for the first time, controlled loading, sympathetic cooling, mass spectrometric identification, and vibrational excitation of ultracold single $HD^+$ ions trapped in a tightly confining radiofrequency trap using single laser-cooled $Be^+$ ions for sympathetic cooling. The apparatus can be used also for preparing other single ions, both lighter and heavier than the coolant ion.

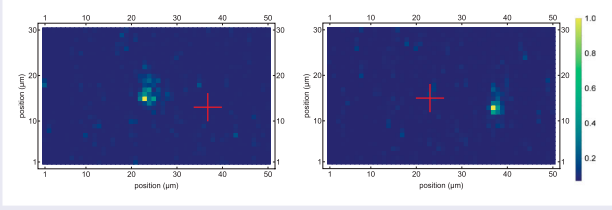


**ARTICLE HISTORY**
Received 17 September 2021
Accepted 29 October 2021

**KEYWORDS**
Single-ion trapping; molecular spectroscopy; sympathetic cooling; molecular hydrogen ion

## 1. Introduction

Trapped ultracold molecular ions are an emerging class of systems allowing highly precise spectroscopic measurements that have relevance in fundamental physics (for a general introduction to low-energy experiments in fundamental physics, see [1,2]). Such measurements enable tests of quantum electrodynamics (QED) of three-body systems [3–5], the determination of some fundamental constants of atomic physics, and searches for physics beyond the Standard Model [4]. As a future perspective, molecular ions could become ideal systems suitable for testing the constancy of the electron-proton mass ratio [6–11].

The fundamental technique for providing the required ultracold molecular ions is the sympathetic cooling of these ions by suitable laser-cooled atomic ions. This technique is very general and powerful, allowing to cool ions of masses 1 u [12] up to masses of several hundred u [13] when applied in the regime where a large number of atomic ions serves as coolant ions ('cluster regime'). Several sympathetically cooled molecular ion species have already been studied spectroscopically by different groups. In the cluster regime, these include the molecular hydrogen ion $HD^+$ (see below), $N_2^+$ [14], $CaH^+$ [15,16], and $SiO^+$ [17].

Following Dehmelt's paradigm of trapping and spectroscopy [18–20] of a single atomic ion, thereby achieving the best control over environmental conditions and permitting internal state detection, a remarkable effort has been undertaken by several groups to establish similar methods for molecular ions. These efforts have been crowned with notable success. The first quantum-optical manipulation of a single molecular ion was performed on an $Mg^+$–$MgH^+$ ion pair. The molecular ion's quantum state was read out, neither destroying the molecule nor its quantum state, by exploiting the strong Coulomb coupling between the two ions [21]. Other investigated two-ion systems, composed of one atomic and one molecular ion, have been $Ca^+$–$CaH^+$ [22] and $Ca^+$–$N_2^+$ [23]. In the former, coherent control and manipulation of molecular

**CONTACT** Christian Wellers christian.wellers@hhu.de

quantum states was demonstrated utilising a variant of quantum logic spectroscopy [24,25]. In the latter, a non-demolition state detection protocol based on coherent motional excitation [26,27] was used. Other systems of interest that bridge the gap between the cluster regime and the two-ion narrative are ion strings composed of two atomic ions and one molecular ion, such as $Ca^+$ and $CaH^+$ in [28].

A fascinating family of molecular ions are the molecular hydrogen ions (MHI). These are the simplest molecules, containing a single electron that binds two singly-charged nuclei. Over the last two decades, the precision physics of MHI has made great advances, with improvements in both experimental and theoretical precision by factors in the order of $10^6$. The precisions have now reached the fractional level of $10^{-11}$–$10^{-12}$ [3–5,29].

Still, there remains a clear potential for further vast improvements. Detailed theoretical studies have predicted that the spectroscopy of MHIs could reach fractional uncertainties at the $10^{-17}$ level [9,10]. Advancing towards this level requires application of the established techniques of atomic ion clocks. So far, the precision spectroscopy experiments on MHIs were performed in the cluster regime. One important shortcoming of these experiments is the destructive internal state detection technique employed: the spectroscopic excitation of molecular ions is detected by dissociating them into two atoms [30]. This approach leads to a very slow rate of acquisition of spectral data, due to the need to repeatedly refilling the coolant ion cluster with molecular ions. Other disadvantages of experimentation on clusters are the incomplete control over micromotion and the presence of inhomogeneous frequency shifts of the molecular ions in the ensemble. Experimentation with a single trapped and motionally well-controlled MHI holds the promise to circumvent these disadvantages and enable substantial further improvements in spectroscopic precision.

In this work, we lay the foundation toward ultra-high resolution, ultra-high precision spectroscopy of single MHIs. We demonstrate stable trapping and sympathetic cooling of a single MHI in a tightly confining linear ion trap, using a single $Be^+$ ion as a coolant ion. The focus is on a simple spectroscopy test experiment on single sympathetically cooled $HD^+$ ions, but the apparatus should be equally suitable for $H_2^+$ or $D_2^+$. Additionally, we also show single-molecular ion trapping of another species, $N_2^+$, in order to demonstrate the flexibility of the apparatus to trap and sympathetically cool molecular ion species that are notably heavier compared to the coolant ion, here by a factor of three. $^{14}N_2^+$ has been identified as a promising candidate for a molecular ion optical clock [8].

The paper is structured as follows: In Section 2 we give a detailed overview of the experimental apparatus. We describe in Section 3 procedures and results on the trapping and laser cooling of the coolant and spectroscopy ions. Section 4 is dedicated to the methods underlying the spectroscopic technique and discussion of the first spectroscopic results. In Section 5 the findings are summarised and an outlook is presented.

## 2. Experimental setup

### 2.1. Concept and overview

The apparatus was designed with the goal of sympathetically cooling a few or a single low-mass ($< 30$ u) molecular ions. In this mass range, molecules are mostly diatomics, but a number of polyatomics are also available, the lightest of which is $H_3^+$. Of particular interest to our work are the MHIs. The non-radioactive members of this family are $H_2^+$, $HD^+$, and $D_2^+$, with masses 2−4 u. Due to its comparatively low mass, $Be^+$ is the only practical atomic ion for sympathetically cooling the MHIs. Concerning the low-mass end of the mass spectrum coolable by $Be^+$ we point out that sympathetic cooling of protons and $H_2^+$ by a laser-cooled $Be^+$ ion cluster has been shown in our group in the past [12,31]. On the high-mass side, an experiment at NIST achieved maintaining a single $Mg^+$ ion (24 u) cold by interaction with a single laser-cooled $Be^+$ ion, after both ions were individually laser-cooled [32].

In order to achieve one-photon spectroscopy without first-order Doppler broadening, the molecular ion confinement in one spatial direction has to be approximately equal to the wavelength of the spectroscopy radiation or smaller (Dicke condition) [33]. For vibrational spectroscopy of $HD^+$ or $H_2^+$ ions, in particular, the wavelengths range from relatively large values, 4–5 μm for the fundamental transitions, to moderately large values for overtone transitions, e.g. 1.4 and 1.1 μm for a fourth- and fifth-overtone transition in $HD^+$, respectively. This regime has recently been explored in the context of molecular ion strings [3] and it has been shown that a resolved carrier transition could be detected and precisely measured.

Beyond the Dicke condition, the quantum Lamb-Dicke regime has been of central importance in quantum optics of trapped atomic and molecular ions. Here, a substantial reduction in the probability of producing recoil effects upon photon absorption is achieved if the classical oscillation frequency of the trapped ion along the direction of the spectroscopy wave exceeds the recoil energy. Equivalently, the wavelength of the spectroscopy radiation should be much larger than the spatial

width of the vibrational ground state wavefunction in the given trap potential. Then, it is possible to suppress the occurrence of a motional vibrational excitation or deexcitation concomitant with the internal excitation of the molecular ion. Considering transition wavelengths as small as 1.1 µm, with a recoil frequency of approximately 50 kHz for $HD^+$, one, therefore, must aim for an ion oscillation frequency of 500 kHz or higher, along the axis parallel to the spectroscopy wave vector. An additional condition for achieving high spectral resolution is that the linewidth of the transition is much smaller than the oscillation frequency. Quite generally, for molecular transitions between rovibrational levels in the electronic ground state, the natural linewidths do satisfy this condition. For example, in $HD^+$, even a high overtone transition such as the fifth overtone exhibits a linewidth of less than 100 Hz.

We designed our apparatus to be able to support different spectroscopy techniques, e.g. destructive detection [30], detection based on applying a near-resonant and therefore internal-state-dependent optical force [21,23,27,34], and quantum logic [22,25].

Figure 1 shows a scheme of the overall system that we have developed. This tabletop setup is capable of producing the required single $Be^+$ ions routinely by photoionisation, and single molecular ions from electron-beam ionisation of a controlled inlet of gas. One of the important aspects in the apparatus layout is to provide optical access for multiple laser beams from multiple directions, not only transverse and under 45°, but also axially. Another goal is to allow imaging with high spatial resolution. For this purpose, the laser-excited $Be^+$ ions can be imaged by a lens mounted close to the trap centre in a reentrant window. Our apparatus is equipped with a set of three pairs of Helmholtz coils that allow a precise control of the magnetic field at the location of the ions. This is important in the precision spectroscopy of MHI, especially if the absolute frequency of the transition is in the mid-infrared or THz range [3,4].

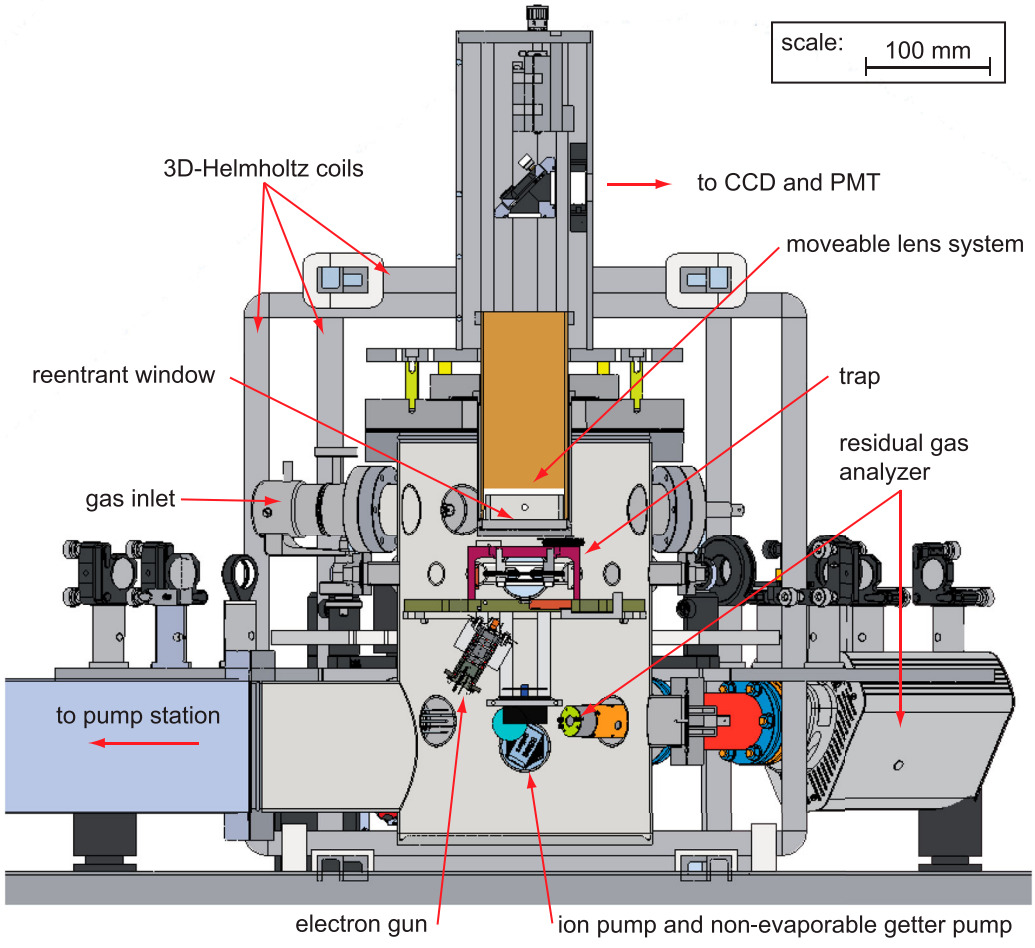


**Figure 1.** Scheme of the vacuum and imaging system. In the shown perspective, the beryllium ovens are not visible. They are located next to the trap.

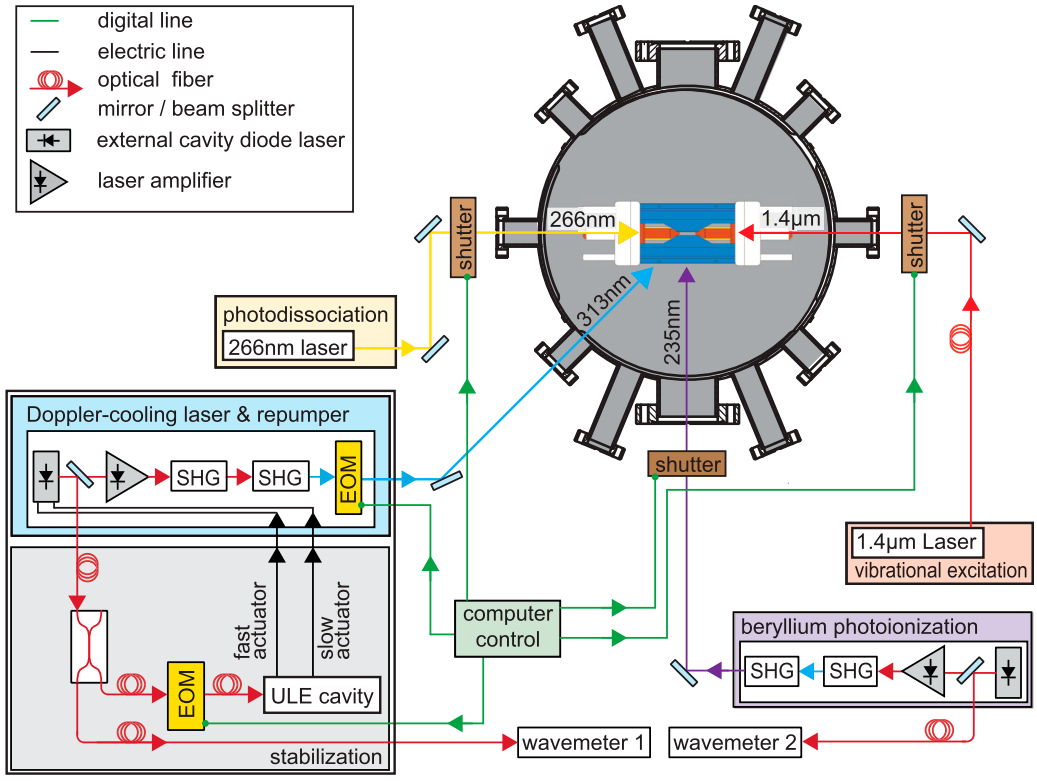


**Figure 2.** Overview of the laser system and the beam irradiation directions into the trap. EOM: electro-optic modulator; SHG: resonant second-harmonic generation; ULE: ultra-low-expansion glass.

The overall system including the lasers is depicted in Figure 2. At the current stage of development and use, there are four laser systems, the $Be^+$ cooling laser (blue) together with its frequency stabilisation unit (grey), the beryllium photoionisation laser (purple), the $HD^+$ vibrational excitation laser (red), and the photodissociation laser (yellow). Power and/or frequencies of all laser waves are computer-controlled (green).

## 2.2. Trapping apparatus

### 2.2.1. The trap

We developed a compact linear radiofrequency (rf) trap suitable for the tight confinement of ions (Figure 3). The design was adapted from a design developed at the Universität Innsbruck. It provides optical access from 13 directions (6 axes plus 1 line of vision) and additional non-optical access for the electron gun, ion detector, oven, etc.

The trap is characterised by short distances from the trap symmetry axis to its quadrupole (blade) electrodes, $r_0 = 0.8\,\text{mm}$, and by a short distance of 2.5 mm from the trap centre to the two axial endcap electrodes. The quadrupole electrodes have half-circular ends with a diameter of 0.4 mm. The ions' confinement is realised by applying dc voltages $U_{\text{ax}}$ to both endcaps (up to 150 V) and an rf modulation with amplitude $U_{\text{rf}}$ (up to 550 V)

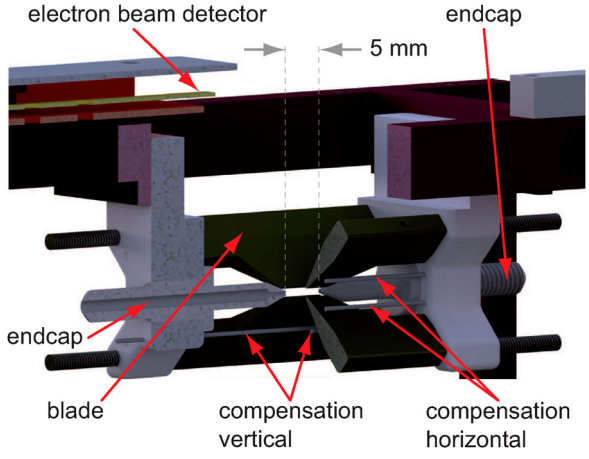


**Figure 3.** The compact rf trap. Dark green: the four quadrupole electrodes (blade electrodes) for the radial confinement. Grey: the axial 'endcap' electrodes for the axial confinement. Also shown in grey are two sets of two rod electrodes for compensating horizontal and vertical displacements of the ions.

at a frequency $\Omega/(2\pi) = 35.9\,\text{MHz}$. We have developed electronics that allows fast switching of these voltages so that the trap's stability parameters can be changed rapidly. This is useful for the purposes of removing undesired ion species from the initially loaded ion crystal, supporting the ion crystallization process, and adjusting the ions' secular frequencies.

### 2.2.2. The vacuum system

The trap is mounted in the vacuum system as shown in Figure 1. The trap size with its numerous optical access directions, including the imaging direction and additional non-optical access for the electron gun, ion detector and two beryllium ovens requires a medium-sized vacuum chamber. We opted for an imaging system located in the air. Because it has to provide high spatial resolution, the required high-quality but bulky objective had to be placed very close to the trap centre, inside a reentrant window.

To achieve an ultra-high vacuum condition with a pressure below $10^{-10}$ mbar, a turbo-molecular pump with a connection flange of 100 mm diameter and an ion pump with additional non-evaporable getter material is used. Additionally, a titanium sublimation pump is occasionally used to remove residual getterable gases and to enhance pumping efficiency. A shutter interfaces the mechanical pumps to the main system, allowing to shut them off, and thereby minimise disturbing vibrations. A quantitative analysis of the composition of the residual background gas is performed on a regular basis using a residual gas analyser.

Two custom-built beryllium ovens are placed close to the trap centre. A slit cover placed 10 mm in front of each oven guides the atomic beam to the trap, avoiding deposition of beryllium on the electrodes. The ovens are attached to a vacuum flange, and therefore can easily be exchanged or maintained by removing the flange.

The alignment of the custom-built electron gun through the trap centre is crucial to avoid an accumulation of stray charges on the trap structure. The alignment can roughly be adjusted by observing a voltage induced by the electron beam on a pair of electrodes placed opposite to the electron gun. One electrode is small, so it provides a signal when hit by electrons passing close to the geometrical trap centre. If the electron beam is misaligned or not well focused, the electrons are detected and blocked by the second large electrode, which also partially protects the reentrant window. To obtain a good alignment, we adjusted the Einzel lens and deflection voltages in the electron gun so as to maximise the voltage appearing on the circuit containing the small electrode, while minimising the voltage on the large-electrode circuit. A fine adjustment is done by observing the effect of the electron beam on a single $Be^+$ ion: a displacement of the ion is induced and observed on the CCD image, if the electron beam hits some parts of the ion trap. If this occurs, the ion position can be reset by the photoionisation laser, as described below (see Section 3.1).

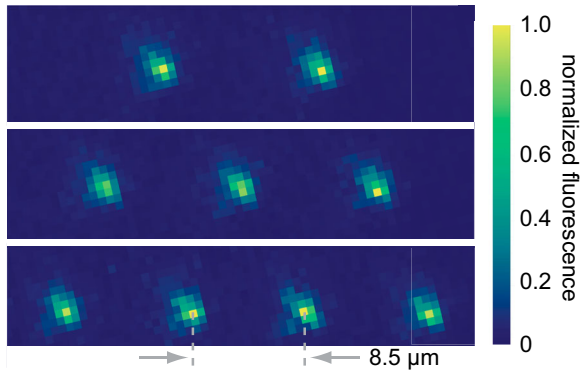


**Figure 4.** CCD image of small ion strings. For these particular images, the 313 nm cooling laser power was set above the saturation intensity. The trap centre is halfway between the outer ions. From a calibration measurement, one pixel corresponds to 0.55(3) µm.

### 2.2.3. The detection system

An objective lens system of 50 mm diameter consisting of five lenses and having a focal length of $f = 36$ mm is mounted at that distance from the stored ions, imaging them to infinity. The objective efficiently collects the ion's fluorescence with a good numerical aperture (compare Figure 1). It is mounted inside a reentrant window that is coated on the vacuum side with indium tin oxide (ITO), so as to minimise the effect of stray charges that reach it. The optical path of the light collected by the objective is divided into two branches by a beam splitter, one going to an intensified CCD camera and the other to a photomultiplier tube (PMT).

The objective magnification is 10. We calibrated the magnification by comparing the image of a beryllium ion string with the ion-ion separation distances calculated from the curvature of the axial potential as determined from the axial secular frequency (see Figure 4).

## 2.3. Laser system

### 2.3.1. Photoionisation laser

Neutral beryllium atoms in the atomic beam are photoionised close to the trap centre by a 235 nm laser beam, in a 2-step excitation process [35]. The radiation is provided by a commercial 470 nm laser that is resonantly frequency-doubled in a custom-built bow-tie cavity containing a beta barium borate (BBO) crystal (Figure 5). The maximum achievable output power is around 12 mW, however, for reliable operation around 5 mW is sufficient.

The 235 nm output power stability is ±10%, as can be seen in Figure 6. This power level is sufficient for loading a single $Be^+$ ion within a few seconds. The 940 nm external cavity diode laser inside the 470 nm laser system is

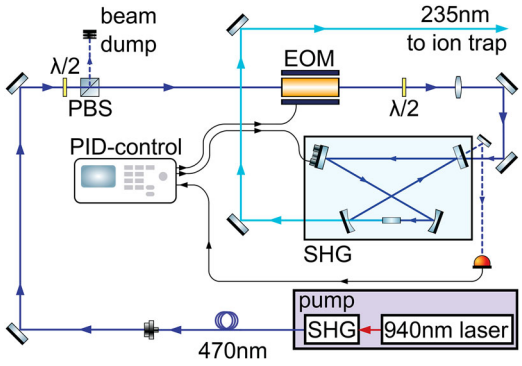


**Figure 5.** Photoionisation laser. PID-control: proportional-integral-derivative servo system that acts on the cavity length. PBS: polarizing beam splitter cube.

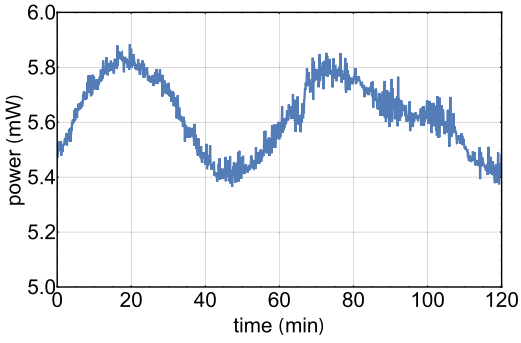


**Figure 6.** Power stability of the beryllium photoionisation laser output (235 nm). Each point plotted is an average of 50 data points measured.

once tuned to the correct atomic transition wavelength. There is no need to control the laser frequency actively since the Doppler broadening of the beryllium transition is large compared to the frequency drift range of the 940 nm laser.

### 2.3.2. Cooling laser

The 313 nm laser for cooling $Be^+$ ions is a commercial resonantly quadrupled amplified diode laser (1252 nm), emitting up to 300 mW at 313 nm. We measured the 1252 nm external cavity diode laser's linewidth by beating against an ultrastable frequency comb. When free-running, the full width at half maximum (FWHM) is approximately 500 kHz.

We have actively frequency-stabilised the 1252 nm laser to an ultra-low expansion (ULE) reference cavity. We use the cavity that was also used in Ref. [36]. For this purpose, a fraction of the laser radiation is phase-modulated by a fibre-coupled waveguide electro-optic modulator (EOM) to imprint sidebands. The modulation frequency is chosen in such a way that the first-order sideband matches the frequency of the TEM00-mode of the reference cavity. A double-modulation technique [37]

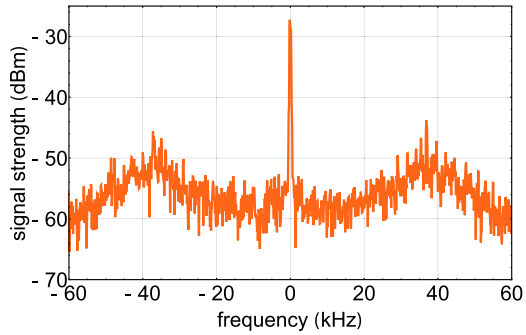


**Figure 7.** Beat of the frequency-stabilised 1252 nm laser with a mode of an optically stabilised frequency comb. The central peak has a linewidth of 0.4 kHz, due entirely to the 1252 nm laser. The resolution bandwidth is 100 Hz.

allows locking the sideband to the cavity, rather than the carrier, and also enables a fine and precise tuning of the laser by adjusting the sideband frequency. The overall sideband tuneability range is 30–800 MHz. Continuous tuning in the locked state is 20 MHz. The $Be^+$ atomic transition resonance happens to be at a modulation frequency of 743 MHz. Figure 7 shows the beat of the stabilised 1252 nm laser with the frequency comb. The linewidth is 0.4 kHz and the drift is negligible. Usually, the laser stays in a lock for a whole working day, even when the sidebands are tuned in 200 kHz steps (corresponding to 800 kHz in the UV).

Laser cooling of $Be^+$ requires a repumper in addition to the Doppler cooling beam. The repumper must be detuned by 1.25 GHz to the red of the actual Doppler cooling transition $^2S_{1/2}(F = 2, m_F = 2) \rightarrow {}^2P_{3/2}(F = 3, m_F = 3)$. These two waves are generated by amplifying and frequency quadrupling the major part of the diode laser wave (1252 nm) and sending the fourth harmonic (313 nm) through a bulk EOM that generates first-order sidebands at 1.25 GHz.

We tune the diode laser frequency such that the (strong) carrier frequency at the fourth harmonic acts as the repumper, depleting the metastable 'dark' state $^2S_{1/2}(F = 1)$ while the blue sideband drives the Doppler cooling transition. By changing the modulation depth, i.e. the rf amplitude applied to the EOM we can easily adjust the power of the Doppler cooling wave. Both repumper and Doppler cooling waves are $\sigma^+$-polarised by a waveplate and injected into the trap at 45° with respect to the trap axis, so as to enable Doppler cooling of the ion in all three degrees of freedom. To reduce the background signal on the PMT due to cooling laser light scattered off the trap components, the laser beam is tightly focused. Its FWHM diameter at the ion's position is 46 μm, measured by recording the variation of the fluorescence intensity along a string of beryllium ions as follows. First, the laser beam's focal spot is aligned to

a single trapped ion to achieve maximum fluorescence. Then additional ions are loaded to form a string. Using the fluorescence levels of the outer ions and their theoretically calculated distances from the trap centre, the FWHM diameter of the laser beam is estimated.

#### 2.3.3. Laser for spectroscopy

For vibrational excitation of the $HD^+$ ion, a commercial 1.4 μm diode laser is employed. Its wavelength can be tuned to the $(\nu = 0, L = 1) \rightarrow (\nu = 4, L = 0)$ transition at 1420 nm. Here, $\nu$ is the vibrational quantum number and $L$ is the rotational quantum number. The laser's linewidth is actively broadened to approximately 50 MHz, allowing to cover all intense hyperfine components of the rovibrational transition. To make sure that the $HD^+$ ion is indeed in the path of the laser beam, the beam is coupled into the trap axially through the endcaps. From theoretical knowledge of the sensitivity of the transition frequency on external fields, we are certain that the frequency shifts from the so far uncontrolled magnetic field or other potential line shifts are well within the linewidth. Using the laser powers measured before the beam enters and after it exits the vacuum system, and approximating the beam waist as the diameter of the holes on the endcap electrodes that guide the laser beam axially, we estimate an intensity of $I_{1420} = 5\,\mathrm{mW/mm^2}$ at the ion's location.

#### 2.3.4. Laser for molecular photodissociation

The photodissociation from the $\nu = 4$ level is performed with a continuous-wave 266 nm laser. The radiation is produced by resonantly doubling 532 nm radiation from a commercial laser in a custom-built cavity. The 266 nm radiation is transported to the trap in free space. The wave is coupled into the trap through the endcap electrodes as well, but counter-propagates with respect to the spectroscopy wave. We infer in the same way as for the spectroscopy laser an intensity of $I_{266} = 60\,\mathrm{mW/mm^2}$ at the ion's position.

## 3. Ion production and laser cooling

### 3.1. Beryllium ion preparation

In order to produce an atomic beam, a current is applied to one of the ovens and ramped up slowly to 0.68 A. After 20 s heat-up time, the photoionisation laser beam is unblocked. A typical power of the 235 nm laser measured behind the vacuum chamber is 4.7 mW. The Doppler cooling laser frequency is red-detuned by 10 MHz (Section 3.3) and the beam power is set to 60 μW. Typically, a single $Be^+$ ion is trapped within 15 s or less, and subsequent ions are loaded every few seconds, using a trap voltage $U_{\mathrm{rf}} = 70\,\mathrm{V}$. Simultaneous loading of two or three ions is observed when the cooling laser frequency is further red-detuned by an additional 4 MHz, the beam power is higher (0.5 mW) and the trap voltage is increased to $U_{\mathrm{rf}} = 100\,\mathrm{V}$.

In order to load a single $Be^+$ ion, the current to the oven is turned off manually and the photoionisation laser beam is blocked as soon as the first ion is observed on the CCD image or PMT. Even if the ion is initially hot and thus cannot be seen on the CCD image, a small increase in fluorescence level can be detected with the PMT and the loading process can be stopped. In the rare cases when two or more $Be^+$ ions are trapped during this procedure, the trap's rf amplitude is subsequently reduced to a value where the quasipotential curvature in one radial direction is smaller than the axial curvature, causing a reorientation of the ion string by 90°, from axial to radial. Now, the ions are no longer in the node line of the rf potential and therefore exposed to higher micromotion heating. In approximately half the applications of this procedure, all but one $Be^+$ ion leave the trap. When this is observed, the trap's rf amplitude is restored to its nominal value.

A single $Be^+$ ion typically remains trapped for several tens of minutes. Repeated loading of $HD^+$ ions using the electron gun (see Section 3.5) results in charging of the trap electrodes and a gradual deterioration in the lifetime of a single $Be^+$ ion is observed. Nevertheless, a maximum storage time of 85 min has been observed for a single $Be^+$ ion which was exposed to several $HD^+$ loading attempts and a total of 16 spectroscopy cycles (see Section 4).

The photoionisation laser at 235 nm also causes reversible charging of the trap electrode. Its effect appears to counteract that of the electron gun. After multiple $HD^+$ loading attempts, a drastic shift in the position of the $Be^+$ ion from the trap centre is observed on the CCD image. In extreme circumstances, a substantial drop in the $Be^+$ ion's fluorescence level is detected in the PMT signal. A short exposure of the trap structure to the photoionisation laser beam appears to restore the ion's position. Therefore, when necessary, we unblock the photoionisation laser beam for 3–5 s prior to a molecular spectroscopy cycle.

### 3.2. Secular excitation

Successful loading and cooling of a single $Be^+$ ion is verified in real time by observing the ion's position and fluorescence level on a CCD camera and on a PMT. Subsequently, an rf signal with an amplitude on the order of millivolts and a frequency sweep around the axial secular frequency $\omega_1$ may be applied to one of the endcap electrodes to excite the ion's axial oscillatory motion.

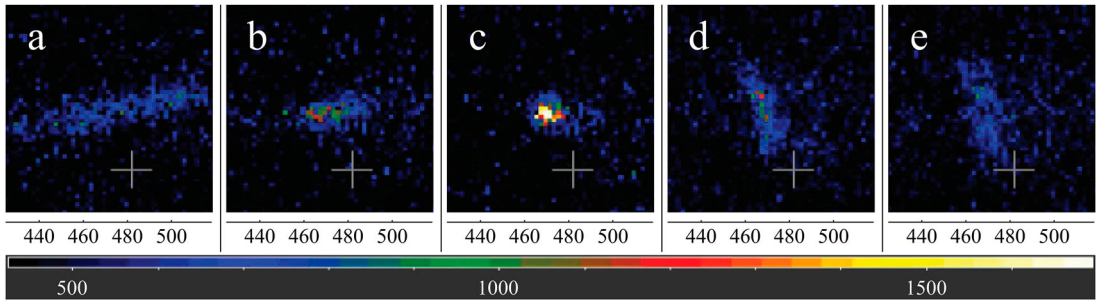


**Figure 8.** Forced axial and radial secular oscillations of a single beryllium ion under typical laser cooling conditions. The centre CCD image (c) shows the ion when no excitation voltage is applied. The amplitude for axial excitation increases from (b) to (a). Panels (d) and (e) show a weak and strong radial excitation, respectively. The axes units are in pixel (0.5 μm). The crosshair cursor in each panel is a reference point. The colour spectrum is the fluorescence signal level.

**Table 1.** Normal modes and eigenfrequencies of an $HD^+$–$Be^+$ pair (predicted) and of a single $Be^+$ ion (measured).

| | | | $HD^+$ | | $^9Be^+$ | | | | |
|---|---|---|---|---|---|---|---|---|---|
| | Mode $\alpha$ | Frequency $\omega_\alpha/(2\pi)$ (kHz) | $e'_{x,\alpha}$ | $e'_{y,\alpha}$ | $e'_{z,\alpha}$ | $e'_{x,\alpha}$ | $e'_{y,\alpha}$ | $e'_{z,\alpha}$ | Mode type |
| Predicted | 6 | 1860.17 | 0.9999 | 0.0000 | 0.0000 | 0.0119 | 0.0000 | 0.0000 | Radial ($x$) in-phase |
| | 5 | 1699.74 | 0.0000 | 0.9999 | 0.0000 | 0.0000 | 0.0143 | 0.0000 | Radial ($y$) in-phase |
| | 4 | 599.93 | 0.0119 | 0.0000 | 0.0000 | −0.9999 | 0.0000 | 0.0000 | Radial ($x$) out-of-phase |
| | 3 | 543.71 | 0.0000 | −0.0143 | 0.0000 | 0.0000 | 0.9999 | 0.0000 | Radial ($y$) out-of-phase |
| | 2 | 532.57 | 0.0000 | 0.0000 | 0.9365 | 0.0000 | 0.0000 | −0.3507 | Axial out-of-phase |
| | 1 | 240.93 | 0.0000 | 0.0000 | 0.3507 | 0.0000 | 0.0000 | 0.9365 | Axial in-phase |
| Measured | 3 | 617.90(70) | | – | | 1 | 0 | 0 | Radial ($x$) |
| | 2 | 563.56(28) | | – | | 0 | 1 | 0 | Radial ($y$) |
| | 1 | 207.1(3.0) | | – | | 0 | 0 | 1 | Axial |

Notes: The frequency values for a single $Be^+$ ion (bottom three rows) are experimentally measured and those for the $HD^+$–$Be^+$ pair are calculated. Here, $e'_{i,\alpha}$, $i = x, y, z$, are the eigenvectors in a mass-weighted coordinate system, defined as $x' = \sqrt{m}\,x$, etc., where $m$ is the mass of the respective particle [38].

When the applied excitation frequency approaches the secular frequency $\omega_1$, the amplitude of the ion's motion increases resulting in an increase in the ion's extent as detected on the CCD camera. Figure 8 shows typical scenarios. The small oscillation amplitudes (cases (b) and (d)) are observable on the CCD image, but are not detectable on the PMT signal – there is almost no change in fluorescence level.

The increased motional energy of the ion also reduces its mean fluorescence level when it is irradiated by the red-detuned Doppler cooling light. This fluorescence is detected by the PMT and represents a signal that can be recorded as a function of the excitation frequency. This procedure will be referred to as a secular scan in the remainder of the paper. Figure 11 (blue) shows a typical secular scan when a single cold beryllium ion is present in the trap. The axial resonance frequency is clearly observed. For an endcap voltage $U_{\mathrm{ax}} = 3\,\mathrm{V}$ the resonance frequency is measured to be $\omega_1(\mathrm{Be}^+)/(2\pi) = 207\,\mathrm{kHz}$ (compare Figure 11, blue data).

Secular scans are also applied when a single $Be^+$ ion is paired with another ion. To interpret the spectrum, it is essential to know the eigenmode frequencies of such a system. They are easily calculated, see e.g. [38]. Generally, the axial potential curvature and the ions' mass and charge are the input parameters that determine the axial single-ion, axial ion-pair and also axial ion-string mode frequencies. Those parameters plus the radial rf pseudopotential curvature then determine the radial eigenfrequencies of ion chains. Conversely, the experimental result for the single-ion $\omega_1(\mathrm{Be}^+)$ provides us with the axial potential curvature and thus we can predict the two axial eigenmode frequencies $\omega_1$, $\omega_2$ of a $Be^+$–$HD^+$ ion pair, see Table 1. From a measurement of the radial single-$Be^+$ secular frequencies, we obtain the radial pseudopotential curvature and can then compute the radial eigenfrequencies of the ion pair. Both the measured single-ion and calculated ion pair frequencies are reported in Table 1.

### 3.3. Micromotion minimisation

In the regime of efficient Doppler cooling (weak intensity) we expect the fluorescence spectral lineshape to be a Lorentzian, whose linewith is due to spontaneous emission, and only a small contribution from power broadening. We indeed find that the spectrum of a single ion is well described by such a profile, see blue data and fit in Figure 9. The fit gives a FWHM of 23 MHz, to be compared to the natural FWHM of 19.4 MHz. This shows that little power broadening is present. In order to achieve

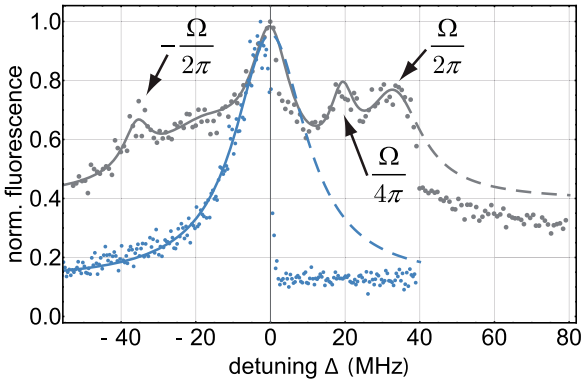


**Figure 9.** Optical resonance of the 313 nm transition of a single laser-cooled beryllium ion. A well-compensated trap shows a clean resonance (blue); in the opposite case (grey), optical sidebands appear. The zero of the indicated detuning values Δ of the cooling laser frequency has been set at the point of maximum fluorescence. Each data point is a 0.1 s average of the PMT signal. The blue line is a Lorentzian fit; the grey line is a fit using 5 Lorentzians.

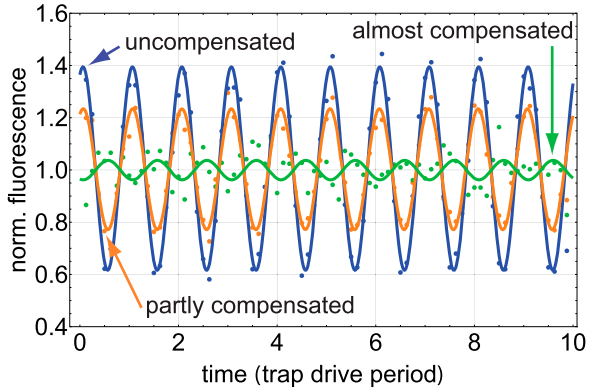


**Figure 10.** Micromotion of a single $Be^+$ ion. Green: in an almost-compensated trap, a micromotion-induced fluorescence modulation does almost not appear in the fluorescence signal. For different settings of the compensation voltages, a modulation is discernible. Orange: partly compensated trap; blue: uncompensated trap. The lines are sinusoidal fits to the data.

the best laser cooling efficiency, we detune the laser frequency to the point of maximum slope of the profile. In this case, it is $\Delta_{opt} = -10$ MHz. As is well-known, when the laser frequency is blue detuned, the ion is heated and the fluorescence drops. In our experiment, the drop is as low as the background PMT counts level and occurs at a detuning very close to that of maximum fluorescence. These observations hold for a well-compensated trap.

If a stray static electric field, especially the stray field caused by the electron beam having charged the electrodes or other parts of the trap structure, is present in the trap centre (i.e. the trap is not well compensated), a single or multiple ions will experience considerable micromotion. This shows up as sidebands in the optical spectrum (grey). The interaction between the ion and the single-frequency cooling laser is now more complex, with a competition of cooling and heating on the various sidebands and carrier taking place. As a result, we find that overall heating of a single ion occurs only when the laser detuning is equal to the blue micromotion sideband at $\Delta = +35.9$ MHz. The seeming appearance of a resonance at $\Omega/4\pi$ is not fully understood and is likely caused by some parametric excitation.

The strength of the micromotion sidebands compared to the mean fluorescence of an ion not experiencing micromotion can be determined also in the time domain [39]. We record the PMT counts with high bandwidth using a field programmable gate array (FPGA). Afterwards, we map the times of photodetection events to the phase of the trap rf drive. In Figure 10 40 s of acquired data are mapped onto 10 trap periods. An uncompensated trap leads to a fluorescence modulation of ±40% (blue). An adjustment of the applied compensation voltages by $\Delta U_{hor} = -0.6$ V and $\Delta U_{ver} = +0.2$ V led to a reduction of modulation by approximately a factor of 2 (orange). For the settings $\Delta U_{hor} = -0.2$ V and $\Delta U_{ver} = +0.2$ V (green) the fluorescence modulation is reduced further to 4(1) %.

The above time-correlation method can be applied to minimise the micromotion amplitude by optimising the compensation voltages. This results in shifting the ion's position to the rf node line and to the axial potential minimum. The ion's position for a well-compensated trap is then marked on the CCD image. When introducing new stray charges or fields e.g. due to electron beam-induced ionisation of HD, a shift of the ion's position and a blurring of its image occurs. In such circumstances, a quick but rough micromotion compensation may be performed, as opposed to a careful measurement of rf-photon correlation described above. This is achieved by altering the compensation voltages and visually controlling the CCD image, with the goal to push the ion back to the marked position on the CCD image. This procedure looks similar to the change from (d) to (c) in Figure 8, with the spatial spread of the $Be^+$ ion image being noticeably reduced.

### 3.4. Ion temperature

The ion's translational temperature may be determined by the method described in ref. [40]. Assuming an ion's spatial distribution as a normal distribution, as one would expect from thermal motion, and neglecting the contribution due to imaging errors of the imaging system (the point spread function), the axial temperature is estimated to be 0.5 mK. Here, the influence of micromotion for oscillations along the trap axis is neglected and the required Gaussian root mean square (RMS) width

is obtained by averaging the fluorescence data collected by the CCD and fitting a Gaussian distribution function to the averaged data. The same procedure is followed also for the radial direction and a temperature of 8 mK is estimated.

### 3.5. Molecular ion preparation

There are two basic approaches to the production of positively charged ions: electron impact ionisation and photoionisation. Laser-induced photoionisation is a 'clean' technique since charging of the surrounding materials can generally be avoided with modest efforts on beam shaping and alignment. The photoionisation of MHI requires a complex laser system tuned to specific wavelengths in the UV region [41–44], but has the advantage of producing the ions in a small range of rovibrational states. Different states can be produced by driving appropriate rovibrational components of electronic transitions.

In contrast, ionisation by electron impact is a very general technique and of great simplicity. Any kind of molecule can be ionised, with the disadvantage of a wide probability distribution in terms of rovibrational levels. This is especially relevant and perhaps problematic in the case of homonuclear diatomic molecular ions (e.g. $H_2^+$, $N_2^+$) in the ground electronic state: the vibrationally excited levels are metastable. Thus, the preparation of such molecules in the ground vibrational state is a challenge, so that electron impact ionisation may have to be complemented by buffer gas cooling [45]. On the contrary, for heteronuclear MHI (e.g. $HD^+$), the lifetime of the excited rovibrational levels is in the order of 10–50 ms (Figure 13). Therefore, within a short time, decay to the ground level $v = 0$ occurs, since blackbody excitation from that level to higher vibrational levels is negligible. However, several rotational levels are occupied under steady-state condition, where spontaneous emission balances blackbody excitation. The steady-state is reached in a few minutes, an acceptable duration in experiments undertaken so far.

The $HD^+$ loading follows the trapping of a single $Be^+$. Referring to Figure 14, the cooling laser power is increased to 150 μW and the trap drive rf amplitude is decreased to $U_{rf} = 40$ V. This corresponds to a level at which species of mass larger than beryllium are not trapped stably or the capturing probability is practically zero. Then, a magnetic field is applied, for the purpose of deflecting the electron beam away from the trap during the electron gun's filament warm-up period. After 8 s, the applied magnetic field is switched off, returning the electron beam to the trap centre. At the same time, a small amount of the molecular gas is introduced by a piezo-electric leak valve, whereby we allow the pressure to rise to $3.8 \times 10^{-10}$ mbar. Since the shutter to the pump station is open, a continuous flow of HD gas is needed. On the CCD camera, a shift in the position of the $Be^+$ ion can be observed, caused by electrode charging effects. As a consequence, the PMT records a decreasing fluorescence.

A trapping event is indicated by a spike in the fluorescence signal. Three cases must be distinguished: (i) the captured ion crystallizes immediately and a jump of the $Be^+$ position can be observed on the CCD, followed by multiple fast position swaps during the sympathetic cooling process. (ii) the captured ion does not crystallize immediately. This indicates more than one captured molecular ion and (iii) the capture failed and the molecular ion is lost. But the $Be^+$ ion position has nevertheless changed and the ion's image spread is larger due to heating effects.

For the cases of successful loading (case i and ii) the $Be^+$–$HD^+$ system needs to be cooled efficiently, for which the following procedures have been experimentally verified. In all cases, the trap rf drive amplitude is slowly increased over the course of a few seconds to restore the nominal value of 70 V. For case (i) the swapping rate decreases and the ions come to rest. The same is true for a previously non-crystallized ion pair. If needed (case ii), the cooling laser power is increased by a factor of 10. If this still does not show any effect, the trap drive amplitude is decreased to 27 V. This leads to a reorientation of the ion pair or string by 90°, from axial to radial, resulting in an ion loss as described in Section 3.1 for beryllium. Alternatively, a 1 to 5 MHz radial secular scan with high amplitude is applied. In this way radial oscillation modes having high amplitudes for the molecular ion are excited. For example, in the case of a two-ion system, as shown in Table 1, this scan would excite the two radial in-phase modes $\omega_5/(2\pi) = 1700$ kHz and $\omega_6/(2\pi) = 1860$ kHz, whose $Be^+$ oscillation amplitudes are 49 and 40 times smaller than the one of $HD^+$, respectively. This will remove some or all molecular ions of the trap.

The effect of this procedure is verified by an axial secular scan (180 to 280 kHz in 30 s). Figure 11 shows in red a typical scan of a $Be^+$–$HD^+$ pair. For the given trap settings, the axial in-phase mode resonance of the $Be^+$–$HD^+$ pair is predicted at $\omega_1/(2\pi) = 241$ kHz, see Table 1; it is measured to be 241.17(30) kHz.

The axial excitation is large enough for the two ions to swap their positions during the scan, before and after the in-phase resonance (but not on-resonance). This is because the scan heats the ion pair, in most cases close to its 'melting point', followed by a re-crystallization that may be accompanied by a swap of ion positions. Figure 12 shows an example. The effect is observable

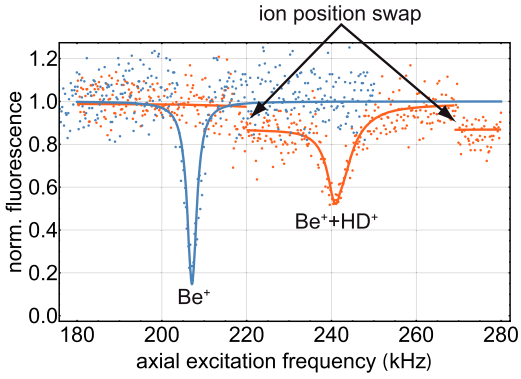


**Figure 11.** Axial in-phase secular scans for a single $Be^+$ ion (blue) and a $Be^+$–$HD^+$ pair (red), measured in different experiments. In the latter case, the ions exchanged their positions twice.

with the PMT, because at the two positions of the $Be^+$ ion a 10% difference in the mean fluorescence level is observed, a change that can be resolved. Usually, the $Be^+$ and $HD^+$ ions do not change places once they are crystallized and no scan is applied. If an axial frequency different from 241 kHz is measured in a secular scan, this indicates that an undesired second ion has been trapped. This ion is therefore removed with the methods explained above.

Sometimes, (case iii), the single $Be^+$ ion's image in the imaging plane is located at one of the two positions of a two-ion string after a failed capture or even after the loss of the molecular ion. This is a result of the charging of trap electrodes by the electron beam. A short exposure of the trap structure to the photoionisation laser restores the ion's original position. We observed that this procedure shrinks the ion's spread, indicating a reduction in heating effects.

## 4. Spectroscopy

The energy levels relevant to this work are displayed in Figure 13. We choose to address a transition that

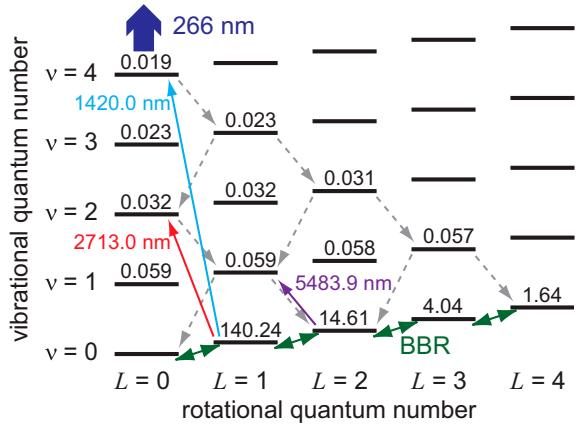


**Figure 13.** Partial rovibrational energy scheme of $HD^+$ (not to scale). In thermal equilibrium, the lower spectroscopy level ($\nu = 0, L = 1$) is populated by 300 K blackbody radiation (BBR, green) that continually induces transitions between the rotational levels of the ground vibrational state. Simultaneously, spontaneous emission processes $L \rightarrow L - 1$ take place (not shown). The lower spectroscopy level can be excited to the level ($\nu = 4, L = 0$) by 1420 nm radiation (light blue). An ion in that upper level can be dissociated by 266 nm radiation (dark blue) or it decays back to the vibrational ground state via spontaneous emission within less than 1 s, reaching first one of the rotational states $L = 0$, 2 or 4. Grey dashed arrows show the dominant spontaneous emission processes. BBR and spontaneous emissions within the $\nu = 0$ manifold eventually lead to occasional population of the lower spectroscopy level $L = 1$. The numbers are the natural lifetimes of the levels, in seconds [46].

starts from the rotational level $L = 1$ in the vibrational ground level because this has the near-maximum theoretical occupation probability in thermal equilibrium, $p(\nu = 0, L = 1) = 0.25$ [47]. We choose ($\nu = 4, L = 0$) as the upper level because the corresponding transition wavelength (1420 nm) is easily available, and because the zero rotational angular momentum simplifies the hyperfine structure. The spectroscopic procedure is portrayed in Figure 14.

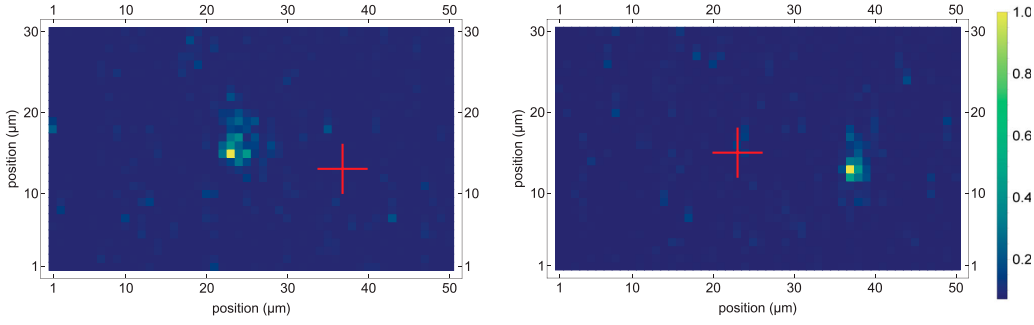


**Figure 12.** CCD images of a $Be^+$–$HD^+$ pair. The $Be^+$ ion can be seen at the two positions of the ion pair. The red cross serves as a guide to the eye and is located at the assumed position of the MHI. The right image is taken after the $HD^+$ ion is loaded. The left image is taken immediately after a position swap has been observed, shortly after a secular excitation scan. 3V are applied both endcaps. The apparent difference in the $Be^+$ ion image extension is attributed to the charging of trap electrodes due to the use of the electron gun for $HD^+$ loading.

After loading and verifying the presence of a single co-trapped $HD^+$ ion by means of a secular scan as described in Section 3.5, the spectroscopy and dissociation lasers irradiate the ion for 10 s. If the ion is in the desired initial level ($v = 0, L = 1$), populated by blackbody radiation (BBR), it can be excited by the spectroscopy laser into the higher rovibrational level ($v = 4, L = 0$). In this case, the dissociation laser excites the ion further into the anti-binding $2p\sigma$ state with essentially unit probability, and the ion dissociates. The theoretical cross section for this process is $8.5 \times 10^{-18}\,\mathrm{cm}^2$ at the wavelength 266 nm [48]. The two dissociation channels $H(1s) + D^+$ or $D(1s) + H^+$ can take place. Only in a fraction of cases, the dissociation of $HD^+$ leads to the observation of a sudden change of the $Be^+$ ion's position on the CCD image (compare Figure 12) as a consequence of the removal of the $HD^+$ ion. We believe that the dissociated fragments of HD sometime react chemically with the residual gas or that a charge exchange takes place. In these events, the newly formed ion remains in the trap. This statement is supported by two observations: (a) a restoration of the $Be^+$ ion's position to the trap centre is not visible on the CCD image, and (b) a subsequent secular excitation scan reveals an unexpected low-frequency resonance indicating the presence of a heavy sympathetically cooled molecular ion.

A quick axial excitation scan of the type shown in Figure 11, but shortened from 30 to 6 s, is applied to verify if the $Be^+$–$HD^+$ pair's in-phase resonance is present or not. If it is absent, this proves that dissociation of the $HD^+$ ion has taken place. If it is still present, both lasers are unblocked for 20 s and a second secular scan is performed afterwards. If the $HD^+$ ion is still trapped, the procedure is repeated for the last time, but now the lasers are unblocked for 30 s.

Afterwards, the molecular ion is removed by applying a strong radial out-of-phase excitation (as discussed in Section 3.5) and a new MHI is loaded into the trap. Then the cycle is repeated. A complete loading - excitation - detection - cleaning cycle has a duration of approximately 2 min.

We performed a total of 18 $HD^+$ preparation and excitation cycles and observed that out of the 18 single $HD^+$ ions, 5 were dissociated in 10 s, 4 in the subsequent 20 s and 4 more in the final 30 s. We also performed the same procedure with the spectroscopy laser detuned by $\Delta_{\mathrm{spec}} = +10\,\mathrm{GHz}$ from the resonance. Out of 9 $HD^+$ single ions none was dissociated in 10 s and none in the subsequent 20 s, but one ion was lost during the last 30 s run. This single observed ion loss is most likely not due to a dissociation event, but rather due to a long storage time of the ion leading to a chemical reaction. Consequently, also for the on-resonance case, such an event could have occurred. A display of these results is shown in Figure 15. For a qualitative understanding of the observation, we compute the normalised excitation rate of the rovibrational transition, using the known transition dipole moment and ignoring the hyperfine structure. The value is $1.4\,\mathrm{s}^{-1}/(\mathrm{mW/mm}^2)$, assuming a gas at 8 mK translational temperature and a laser spectrum narrower than the Doppler width of 4 MHz. We estimate that the effect of the hyperfine structure present and the actual laser linewidth yields an effective excitation rate reduced by a factor of the order $10^2$, the product

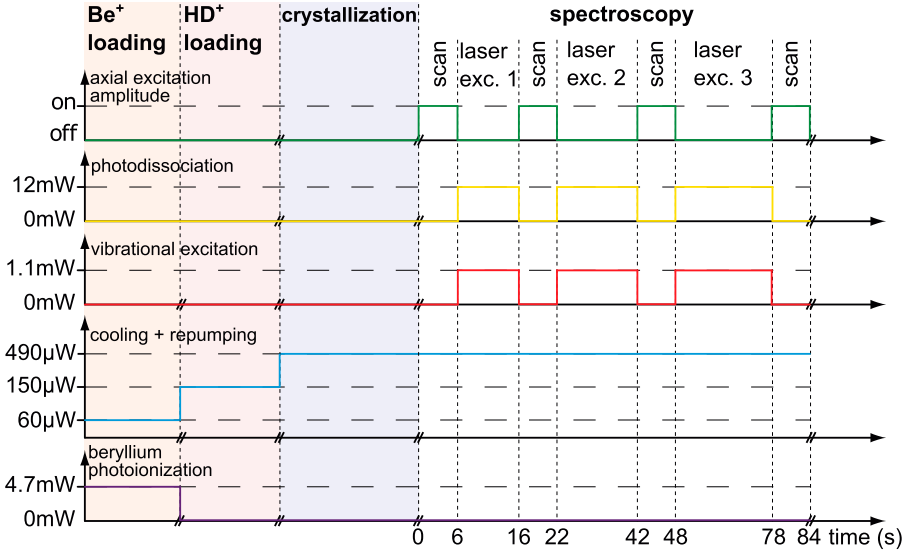


**Figure 14.** Timing diagram for the spectroscopy on single $HD^+$ ions. The spectroscopy laser (red) and the dissociation laser (yellow) simultaneously irradiate the $HD^+$ ion for 10 s, then 20 s and finally 30 s. Before and after each irradiation period a secular scan (green) is performed to probe whether the single $HD^+$ is still present or not.

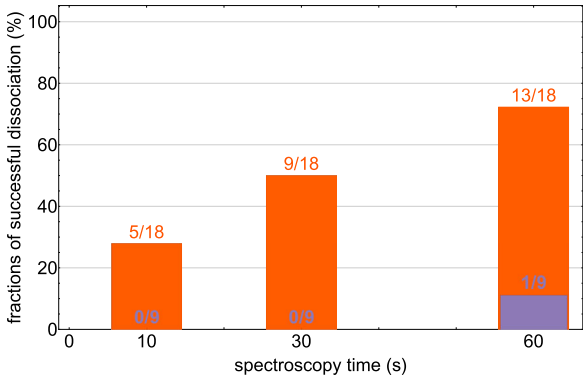


**Figure 15.** Results of vibrational excitation – dissociation of a set of single $HD^+$ ions. The three columns show the cumulated fractions of successful $HD^+$ ion dissociations after 10, 30 and 60 s of cumulative irradiation time by the 1420 nm and 266 nm lasers, respectively. Orange: the spectroscopy laser is tuned to resonance, the ion loss is significant. Blue: the spectroscopy laser is detuned by +10 GHz. The one event that occurred within the last 30 s might be due to a reaction with residual gas in the vacuum chamber during the relatively long storage time of this specific ion.

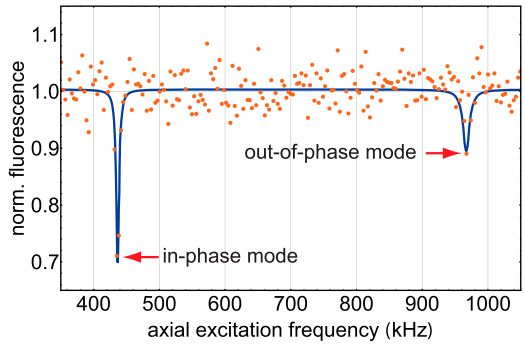


**Figure 16.** Typical axial frequency spectrum of a $Be^+$–$N_2^+$ ion pair. The first resonance is the in-phase axial mode, the second is the out-of-phase mode. Scan duration: 30 s. The blue line is a guide to the eye.

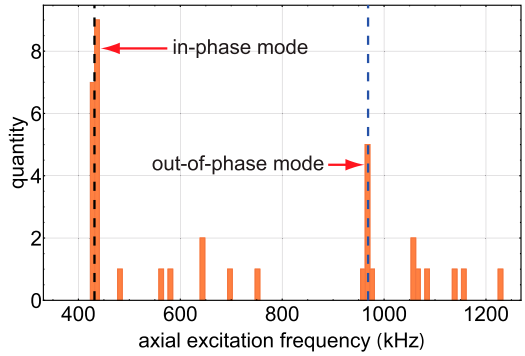


**Figure 17.** Histogram of $Be^+$–$N_2^+$ ion-pair axial resonance frequencies as observed during a number of scans. The theoretically predicted values for the axial in-phase (black, $\omega_1$) and axial out-of-phase (blue, $\omega_2$) modes are indicated by dashed lines.

of the number of hyperfine components (10) and the ratio of laser linewidth to Doppler width (12). Given the above value of $I_{1420}$ this leads to an excitation rate of $\approx 0.07\ s^{-1}$ if the molecules are in the initial level. Since the thermal population fraction of that state is 0.25, after a 10 s irradiation, the ensemble-averaged cumulative excitation probability is $\approx 0.2$. The observed excitation probabilities are in rough agreement with this simple estimate. The action of the excitation lasers on single molecular ions is convincing. Due to the facts that the vibrational excitation laser intensity is low and that the $HD^+$ ions are not prepared and do not permanently stay in the initial spectroscopy level, a time-dependent cumulative dissociation probability is observed.

### 4.1. Other ion species

The apparatus features the ability to trap various ion species that can be sympathetically cooled by the atomic ion. As an example, a $Be^+$–$N_2^+$ ion pair is prepared as follows.

We first prepare a single $Be^+$ in the trap and measure its axial ($\omega_1/(2\pi) \approx 652$ kHz) and radial ($\omega_2/(2\pi) \approx 1.665$ MHz and $\omega_3/(2\pi) \approx 1.673$ MHz) secular frequencies by applying excitation scans as described above. Using these values, we compute the eigenfrequencies of the $Be^+$–$N_2^+$ system, in the same way as done for the $Be^+$–$HD^+$ system.

An $N_2^+$ ion is loaded in a similar way as an $HD^+$ ion and excitation scans are performed. A typical scan result is shown in Figure 16. The PMT signal (red dots, normalised) and the corresponding fit to the data (solid blue line) show the axial in-phase resonance $\omega_1/(2\pi) \approx 436.7$ kHz and the axial out-of-phase resonance $\omega_2/(2\pi) \approx 967.1$ kHz. The axial out-of-phase resonance is less efficiently excited because the lighter ion ($Be^+$) oscillates with a smaller amplitude than in the in-phase mode (see Table 1). This results in a signal on the PMT that is almost hidden in the noise, but was confirmed by a clearly visible excitation on the CCD camera (comparable to Figure 8(b)), as discussed above. The results of the resonances observed in a number of scans are gathered in a histogram (Figure 17).

A comparison of the measured frequencies with the calculated frequencies $\omega_1/(2\pi) \approx 431.5$ kHz and $\omega_2/(2\pi) \approx 986.9$ kHz, proves the dark ion to be $N_2^+$. The histogram Figure 17 also contains unknown resonances. These can be explained by random position changes or collisions with residual gas occurring during the scans.

## 5. Discussion and conclusions

A system suited for a range of quantum-optical studies on various single molecular ions has been designed, built and characterised. At present, single $HD^+$- and single $N_2^+$- ions are reliably prepared in the trap, where they are sympathetically cooled to sub-millikelvin axial secular temperatures. Current storage times for the single molecular ions are already sufficiently long for permitting precision spectroscopic studies.

A proof of the overall functionality is given by demonstrating the induction and detection of a vibrational transition on single MHIs. The initial state is a thermally populated rotational state that is excited to a higher rovibrational state by a continuous-wave laser and then photodissociated. The photodissociation is verified by careful observation of the ion positions and analysis of the secular excitation scans. We find evidence of chemical reaction or charge exchange of $HD^+$ fragments with the residual gas, resulting in the co-trapping of an unwanted heavier molecular ion species. We do not observe that the fragments $H^+$ or $D^+$ remain trapped together with the beryllium ion.

Towards the implementation of high-precision spectroscopy of a single MHI, it is important to improve the probability that the prepared single ion is in the desired initial state for spectroscopy. For the heteronuclear $HD^+$ molecule this can be done via rotational cooling [47] (red and purple arrows in Figure 13), a technique well-established in our laboratory, while for the homonuclear $H_2^+$ molecule other techniques have to be applied, for example selective photodissociation of those ions that are in unwanted vibrational states. A more advanced preparation is hyperfine state preparation [49], a technique that still requires more development. The availability of such techniques will shorten the data acquisition time, improve the data statistics, and allow application of certain types of nondestructive internal state read out.

We believe that once rotational cooling is implemented, the apparatus could in principle be used for precision spectroscopy on single molecular hydrogen ions, achieving precision at the $10^{-13}$ fractional level with acceptable effort. Two reasons for this are that (i) accurate theoretical predictions for the transition frequencies are already available and therefore the transitions do not need to be searched for over substantial frequency intervals, and (ii) the excitation spectrum of a transition will exhibit an ultra-narrow resolved carrier component, as can be inferred from our observations with $HD^+$ ion strings in a beryllium cluster. Based on our results in Section 4, we find that with approximately 20 single-ion preparation and excitation cycles we can obtain one data point of the spectrum (excitation probability) with reasonable signal-to-noise ratio. We expect that we can enhance the system performance so as to obtain two data points per day. Thus, one transition line can be measured within one week, with an expected linewidth at the $10^{-13}$ fractional level. Our past experience in characterising systematics indicates that a line needs to be measured half-a-dozen times in order to verify the systematic shifts, by varying in succession magnetic field, spectroscopy laser power, trap rf amplitude, and cooling laser intensity by a factor of two. Altogether, within a two-month period the transition frequency of a suitably chosen Zeeman component of a rovibrational transition could be determined with a fractional uncertainty lower than $10^{-12}$.

An important question is how thight the confinement of the MHI is for the conditions realised in the apparatus at present. With the current observation tools, the CCD camera with its 200 ms exposure time, and the PMT with its signal noise level (10%), we find no indication that there is significant spurious large-amplitude motion of the $Be^+$–$HD^+$ system. The spatial extent of the $Be^+$ ion CCD image is 0.5 μm in the two observed directions, corresponding to a temperature upper limit of 8 mK. Assuming the same temperature for the $HD^+$ and $Be^+$ ion, we can then place an upper limit to the $HD^+$ motional range of $< 1\,\mu$m in each direction. Thus, for the 5.1 μm-wavelength fundamental transition the Dicke condition $kx_{\mathrm{RMS}} \lesssim 1$ is satisfied and a substantial recoil-free carrier transition is expected. Possibly, sideband cooling on the $(\nu = 0, L = 1) \rightarrow (\nu = 1, L = 0)$ vibrational transition will be feasible.

Finally, we point out that a major improvement in MHI spectroscopy would be the introduction of a nondestructive state detection technique that consequently allows to reuse the same molecular ion for multiple spectroscopy cycles, effectively reducing the spectroscopic data acquisition time. This will also reduce the number of loading events and hence the total experimentation time. Evidence that a heteronuclear MHI in an MHI-$Be^+$ ion pair is in a particular rovibrational state should be obtainable by coherently exciting the motion of the ion pair using an intense standing-wave near-resonantly tuned to a fundamental or low-overtone vibrational transition [23,34]. A suitable laser for this purpose appears to be a high-power continuous-wave optical parametric oscillator.

## Acknowledgments

The authors are grateful to Prof. Johannes Hecker Denschlag's group (Universität Ulm) for providing their trap's CAD files.

We are indebted to M. G. Hansen for his assistance on frequency stabilisation of the Doppler cooling laser, to S. Alighanbari for his help with the $HD^+$ spectroscopy and photodissociation lasers, and to both for their insights and stimulating discussions. M.S., G.G. and C.W. acknowledge a fellowship from the Professor W. Behmenburg-Schenkung.

## Disclosure statement

No potential conflict of interest was reported by the author(s).

## Funding

This work has received funding from the European Research Council (ERC) under the European Union's Horizon 2020 research and innovation programme (grant agreement number 786306, 'PREMOL'), and from the Deutsche Forschungsgemeinschaft and Land Nordrhein-Westfalen in projects INST 208/667-1 FUGG and INST 208/737-1 FUGG. K. B. acknowledges support from the Alexander von Humboldt Foundation for a fellowship under Humboldt-ID 1159544.

## ORCID

*Christian Wellers* http://orcid.org/0000-0001-6084-6495
*Magnus R. Schenkel* http://orcid.org/0000-0001-6048-9168
*Gouri S. Giri* http://orcid.org/0000-0002-6713-4412
*Kenneth R. Brown* http://orcid.org/0000-0001-7716-1425
*Stephan Schiller* http://orcid.org/0000-0002-0797-8648

## References

[1] M.S. Safronova, D. Budker, D. DeMille, D.F.J. Kimball, A. Derevianko and C.W. Clark, Rev. Mod. Phys **90**, 025008 (2018). doi:10.1103/RevModPhys.90.025008
[2] D. DeMille, J.M. Doyle and A.O. Sushkov, Science **357** (6355), 990–994 (2017). doi:10.1126/science.aal3003
[3] I.V. Kortunov, S. Alighanbari, M.G. Hansen, G.S. Giri, V.I. Korobov and S. Schiller, Nat. Phys. **17**, 59–573 (2021). doi:10.1038/s41567-020-01150-7
[4] S. Alighanbari, G.S. Giri, F.L. Constantin, V.I. Korobov and S. Schiller, Nature **581**, 152–158 (2020). doi:10.1038/s41586-020-2261-5
[5] S. Patra, M. Germann, J.P. Karr, M. Haidar, L. Hilico, V.I. Korobov, F.M.J. Cozijn, K.S.E. Eikema, W. Ubachs and J.C.J. Koelemeij, Science **369**, 1238 (2020). doi:10.1126/science.aba0453
[6] D. Hanneke, R.A. Carollo and D.A. Lane, Phys. Rev. A **94**, 050101 (2016). doi:10.1103/PhysRevA.94.050101
[7] K. Beloy, M.G. Kozlov, A. Borschevsky, A.W. Hauser, V.V. Flambaum and P. Schwerdtfeger, Phys. Rev. A **83**, 062514 (2011). doi:10.1103/PhysRevA.83.062514
[8] M. Kajita, G. Gopakumar, M. Abe, M. Hada and M. Keller, Phys. Rev. A **89**, 032509 (2014). doi:10.1103/PhysRevA.89.032509
[9] J.P. Karr, J. Mol. Spectrosc. **300**, 37–43 (2014). doi:10.1016/j.jms.2014.03.016
[10] S. Schiller, D. Bakalov and V.I. Korobov, Phys. Rev. Lett **113**, 023004 (2014). doi:10.1103/PhysRevLett.113.023004
[11] S. Schiller and V. Korobov, Phys. Rev. A **71**, 032505 (2005). doi:10.1103/PhysRevA.71.032505
[12] P. Blythe, B. Roth, U. Fröhlich, H. Wenz and S. Schiller, Phys. Rev. Lett **95**, 183002 (2005). doi:10.1103/PhysRevLett.95.183002
[13] A. Ostendorf, C.B. Zhang, M.A. Wilson, D. Offenberg, B. Roth and S. Schiller, Phys. Rev. Lett. **97**, 243005 (2006). doi:10.1103/PhysRevLett.97.243005
[14] M. Germann, X. Tong and S. Willitsch, Nat. Phys. **10**, 820–824 (2014). doi:10.1038/nphys3085
[15] A.T. Calvin, S. Janardan, J. Condoluci, R. Rugango, E. Pretzsch, G. Shu and K.R. Brown, J. Phys. Chem. A **122**, 3177–3181 (2018). doi:10.1021/acs.jpca.7b12823
[16] A.T. Calvin and K.R. Brown, J. Phys. Chem. Lett. **9** (19), 5797–5804 (2018). doi:10.1021/acs.jpclett.8b01387PMID: 30212222.
[17] P.R. Stollenwerk, I.O. Antonov, S. Venkataramanababu, Y.W. Lin and B.C. Odom, Phys. Rev. Lett. **125**, 113201 (2020). doi:10.1103/PhysRevLett.125.113201
[18] H.G. Dehmelt, Bull. Am. Phys. Soc. **8**, 23 (1963).
[19] H.G. Dehmelt, Bull. Am. Phys. Soc. **7**, 470 (1962).
[20] H.G. Dehmelt, Phys. Rev. **103**, 1125–1126 (1956). doi:10.1103/PhysRev.103.1125
[21] F. Wolf, Y. Wan, J. Heip, F. Gebert, C. Shi and P. Schmidt, Nature **530**, 457–460 (2016). doi:10.1038/nature16513
[22] C. Chou, C. Kurz, D. Hume, P. Plessow, D.R. Leibrandt and D. Leibfried, Nature **545**, 203–207 (2017). doi:10.1038/nature22338
[23] M. Sinhal, Z. Meir, K. Najafian, G. Hegi and S. Willitsch, Science **367**, 1213–1218 (2020). doi:10.1126/science.aaz9837
[24] Y. Wan, F. Gebert, J.B. Wübbena, N. Scharnhorst, S. Amairi, I.D. Leroux, B. Hemmerling, N. Lärch, K. Hammerer and P.O. Schmidt, Nat. Commun. **5**, 3096 (2014). doi:10.1038/ncomms4096
[25] P.O. Schmidt, T. Rosenband, C. Langer, W.M. Itano, J.C. Bergquist and D.J. Wineland, Science **309**, 749–752 (2005). doi:10.1126/science.1114375
[26] J.C.J. Koelemeij, B. Roth and S. Schiller, Phys. Rev. A **76**, 023413 (2007). doi:10.1103/PhysRevA.76.023413
[27] D.B. Hume, C.W. Chou, D.R. Leibrandt, M.J. Thorpe, D.J. Wineland and T. Rosenband, Phys. Rev. Lett. **107**, 243902 (2011). doi:10.1103/PhysRevLett.107.243902
[28] N.B. Khanyile, G. Shu and K.R. Brown, Nat. Commun. **6**, 7825 (2015). doi:10.1038/ncomms8825
[29] V.I. Korobov, L. Hilico and J.P. Karr, Phys. Rev. Lett. **118**, 233001 (2017). doi:10.1103/PhysRevLett.118.233001
[30] B. Roth, J.C.J. Koelemeij, H. Daerr and S. Schiller, Phys. Rev. A **74**, 040501 (2006). doi:10.1103/PhysRevA.74.040501
[31] B. Roth and S. Schiller, in *Cold Molecules: Theory, Experiment, Applications*, edited by W.C. Stwalley, B. Friedrich, and R. Krems (CRC Press, Boca Raton, 2009).
[32] M.D. Barrett, B. DeMarco, T. Schaetz, V. Meyer, D. Leibfried, J. Britton, J. Chiaverini, W.M. Itano, B. Jelenković, J.D. Jost, C. Langer, T. Rosenband and D.J. Wineland, Phys. Rev. A **68**, 042302 (2003). doi:10.1103/PhysRevA.68.042302
[33] R.H. Dicke, Phys. Rev. **89**, 472–473 (1953). doi:10.1103/PhysRev.89.472
[34] J.C.J. Koelemeij, B. Roth, A. Wicht, I. Ernsting and S. Schiller, Phys. Rev. Lett. **98**, 173002 (2007). doi:10.1103/PhysRevLett.98.173002

[35] H.Y. Lo, J. Alonso, D. Kienzler, B.C. Keitch, L.E. de Clercq, V. Negnevitsky and J.P. Home, Appl. Phys. B **114**, 17–25 (2013). doi:10.1007/s00340-013-5605-0
[36] M.G. Hansen, E. Magoulakis, Q.F. Chen, I. Ernsting and S. Schiller, Opt. Lett. **40**, 2289–2292 (2015). doi:10.1364/OL.40.002289
[37] A.Y. Nevsky, S. Alighanbari, Q. Chen, I. Ernsting, S. Vasilyev, S. Schiller, G. Barwood, P. Gill, N. Poli and G.M. Tino, Opt. Lett. **38**, 4903–6 (2013). doi:10.1364/OL.38.004903
[38] J.P. Home, Adv. At. Mol. Opt. Phys., **62**, 231–277 (2013). doi:10.1016/B978-0-12-408090-4.00004-9
[39] D.J. Berkeland, J.D. Miller, J.C. Bergquist, W.M. Itano and D.J. Wineland, J. Appl. Phys. **83**, 5025–5033 (1998). doi:10.1063/1.367318
[40] S. Knünz, M. Herrmann, V. Batteiger, G. Saathoff, T.W. Hänsch and T. Udem, Phys. Rev. A **85**, 023427 (2012). doi:10.1103/PhysRevA.85.023427
[41] J. Schmidt, T. Louvradoux, J. Heinrich, N. Sillitoe, M. Simpson, J.P. Karr and L. Hilico, Phys. Rev. Appl. **14**, 024053 (2020). doi:10.1103/PhysRevApplied.14.024053
[42] S.T. Pratt, Rep. Prog. Phys. **58** (8), 821–883 (1995). doi:10.1088/0034-4885/58/8/001
[43] M.A. O'Halloran, S.T. Pratt, P.M. Dehmer and J.L. Dehmer, J. Chem. Phys. **87**, 3288–3298 (1987). doi:10.1063/1.453022
[44] P.M. Dehmer and W.A. Chupka, J. Chem. Phys. **79** (4), 1569–1580 (1983). doi:10.1063/1.446029
[45] S. Schiller, I. Kortunov, M. Hernández Vera, F. Gianturco and H. da Silva, Phys. Rev. A **95**, 043411 (2017). doi:10.1103/PhysRevA.95.043411
[46] Z. Amitay, D. Zajfman and P. Forck, Phys. Rev. A **50**, 2304–2308 (1994). doi:10.1103/PhysRevA.50.2304
[47] T. Schneider, B. Roth, H. Duncker, I. Ernsting and S. Schiller, Nat. Phys. **6**, 275–278 (2010). doi:10.1038/nphys1605
[48] M. Tadjeddine and G. Parlant, Mol. Phys. **33**, 1797–1803 (1977). doi:10.1080/00268977700101461
[49] U. Bressel, A. Borodin, J. Shen, M. Hansen, I. Ernsting and S. Schiller, Phys. Rev. Lett. **108**, 183003 (2012). doi:10.1103/PhysRevLett.108.183003